RESEARCH ARTICLE | OCTOBER 09 2023

Electronic and nanoscale structures of metal oxyhalide intergrowth photocatalysts Θ

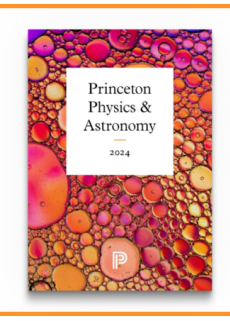
Kaustav Chatterjee ⁽ⁱ⁾; Jared Stanley ⁽ⁱ⁾; Vinayak P. Dravid ⁽ⁱ⁾; Roberto dos Reis ⁽ⁱ⁾; Sara E. Skrabalak ⁽ⁱ⁾



Appl. Phys. Lett. 123, 154101 (2023) https://doi.org/10.1063/5.0159761







Browse our new Physics and Astronomy Catalog 30% off titles with code **P326**





Electronic and nanoscale structures of metal oxyhalide intergrowth photocatalysts

Cite as: Appl. Phys. Lett. **123**, 154101 (2023); doi: 10.1063/5.0159761 Submitted: 26 May 2023 · Accepted: 23 September 2023 · Published Online: 9 October 2023







Kaustav Chatterjee, Dared Stanley, DVinayak P. Dravid, Roberto dos Reis, Skala and Sara E. Skrabalak D

AFFILIATIONS

- ¹Department of Chemistry, Indiana University, Bloomington, Indiana 47405, USA
- ²Department of Materials Science and Engineering, Northwestern University, Evanston, Illinois 60208, USA
- ³The NUANCE Center, Northwestern University, Evanston, Illinois 60208, USA
- ⁴International Institute of Nanotechnology, Northwestern University, Evanston, Illinois 60208, USA

ABSTRACT

Multimetal oxyhalide intergrowths show promise for photocatalytic water splitting. However, the relationships between intergrowth stoichiometry and their electronic and nanoscale structures are yet to be identified. This study investigates $Bi_4TaO_8Cl-Bi_2GdO_4Cl$ intergrowths and demonstrates that stoichiometry controls the tilting of $[TaO_6]$ octahedra, influencing the bandgap of the photocatalyst and its valence and conduction band positions. To determine how the $[TaO_6]$ octahedral tilting in the intergrowths manifests as a function of intergrowth stoichiometry, we investigated changes in crystal symmetry by analyzing features arising at the higher order Laue zone (HOLZ) of convergent-beam electron diffraction patterns. Higher Ta content intergrowths displayed a more intense outer HOLZ ring compared to lower Ta content intergrowths, indicating transformation from $P2_1cn$ (orthorhombic) to P4/mmm (tetragonal). This finding suggests that more distortion occurs along the $\langle 001 \rangle$ directions of the crystal than the $\langle 100 \rangle$ and $\langle 010 \rangle$ directions. This variation directly impacts the electronic structure, affecting both conduction and valence band energy levels. By combining ultraviolet photoelectron spectroscopy, UV-visible diffuse reflectance spectroscopy, and electron energy loss spectroscopy, the absolute band positions of the intergrowths were determined. Agreement between the bandgaps obtained via ensemble and nanoscale measurements indicates nanoscale homogeneity of the electronic structure. Overall, the integrated approach establishes that the bandgap energy increases with increasing Ta content, which is correlated with the crystal symmetry and $[TaO_6]$ octahedral tilting. Broadly, the modular nature of intergrowths provides building block layers to tune octahedral tilting within perovskite layers for manipulation of optoelectronic properties.

Published under an exclusive license by AIP Publishing. https://doi.org/10.1063/5.0159761

Solar photocatalytic water splitting is a promising renewable energy technology. $^{1.2}$ Bismuth-based oxyhalides, such as $\mathrm{Bi_4MO_8X}$ (M = Ta, Nb; X = Cl, Br), are a new class of durable photocatalysts capable of harvesting visible light. These materials consist of alternating layers of perovskite $[\mathrm{MO_4}]^{3-}$, halide $[\mathrm{X}]^{-}$, and two $[\mathrm{Bi_2O_2}]^{2+}$ blocks. $^{3-5}$ Introducing additional metal perovskite layers or substituting atoms in these materials can further tune their optoelectronic properties. $^{6.7}$ However, investigating the relationships between crystal structure and key properties in complex photocatalytic materials remains challenging. Understanding how the crystal structures of these complex metal heteroanionic materials give rise to their electronic structures and can be modulated is essential for material design. 8

Recently, the Skrabalak group reported durable Bi₄TaO₈Cl-Bi₂GdO₄Cl intergrowths for visible-light-responsive water splitting.

These intergrowths exhibited a tunable bandgap that increases as the Ta:Gd molar ratio (Ta%) increased and overall water splitting was achieved using a Z-scheme, with high material durability. Moreover, the intergrowths displayed greater photocatalytic activity than the parent materials (Bi₄TaO₈Cl or Bi₂GdO₄Cl), with the Ta 50% sample having the highest activity for the oxygen evolution reaction (OER). Although prior studies have measured octahedral tilting in other perovskite structures, no such studies have been reported for metal oxyhalides with layered perovskite structures. Furthermore, there are limited reports on determining the absolute energy levels of conduction and valence bands of metal oxyhalides with layered perovskite structures. In this manuscript, the absolute energy levels and band edges of Bi₄TaO₈Cl–Bi₂GdO₄Cl intergrowths were determined using ensemble (bulk) as well as nanoscale characterization techniques, along

^{a)}Authors to whom correspondence should be addressed: roberto.reis@northwestern.edu and sskrabal@indiana.edu

with characterization of the crystal symmetry, which is correlated with the octahedral tilting of the perovskite layers and its effect on the overall electronic structures.

Specifically, convergent-beam electron diffraction (CBED) was used to analyze the octahedral tilting of the [TaO₆] in the Bi₄TaO₈Cl-Bi₂GdO₄Cl intergrowths composed of flexible [TaO₆] octahedral layers and rigid [GdO₈] layers. CBED provides precise information about the symmetry elements and local lattice constants, thereby allowing a study of the crystal symmetry and its effects on the octahedral tilting in the intergrowth photocatalyst. To accurately measure the band energy levels and the overall band structure of Bi₄TaO₈Cl-Bi₂GdO₄Cl intergrowths, ultraviolet photoelectron spectroscopy (UPS) and UV-visible diffuse reflectance spectroscopy (DRS) were used. The optical bandgap can be calculated by DRS, and the positions of the Fermi and valence band energy levels can be determined from the UPS studies. Combining these results, the conduction band energy level can be calculated with respect to vacuum. Additionally, electron energy-loss spectroscopy (EELS) was used to determine the nanoscale electronic structure and correlate the bandgap values obtained from DRS (ensemble measurement). Overall, this manuscript establishes that the bandgap energy increases with increasing Ta content, which is correlated with the changes in crystal symmetry and [TaO₆] octahedra tilting in the Bi₄TaO₈Cl-Bi₂GdO₄Cl

intergrowth structure. Such insight should facilitate the future intergrowth design given their modular nature.

The intergrowth samples are named as Ta *X* %, where *X* denotes the relative percentage of Bi₄TaO₈Cl in the Bi₄TaO₈Cl-Bi₂GdO₄Cl intergrowth phases with respect to the initial Ta₂O₅/Gd₂O₃ molar ratio (see supplementary material for details of their synthesis and general analytical methods). As reported previously, the final samples have stoichiometries that align closely with the initial molar ratio. Bi₂GdO₄Cl has a tetragonal crystal structure exhibiting the *P4/mmm* space group, while Bi₄TaO₈Cl has an orthorhombic crystal structure exhibiting space group *P2*₁*cn*. He intergrowths were examined with the high spatial resolution offered by CBED to identify the changes in the crystal structure as such changes are strongly connected to changes in an electronic structure.

The transformation from orthorhombic $P2_1cn$ to tetragonal P4/mmm involves a significant change in the symmetry elements of the crystal lattice. Specifically, P4/mmm exhibits three mutually perpendicular twofold rotation axes, four mirror planes, and four glide planes, while $P2_1cn$ contains only one twofold rotation axis, two mirror planes, and two glide planes (Fig. 1). The transformation also eliminates the center of inversion present in $P2_1cn$. These changes reflect a higher degree of symmetry and periodicity in P4/mmm. The higher degree of symmetry and periodicity in the P4/mmm space group is

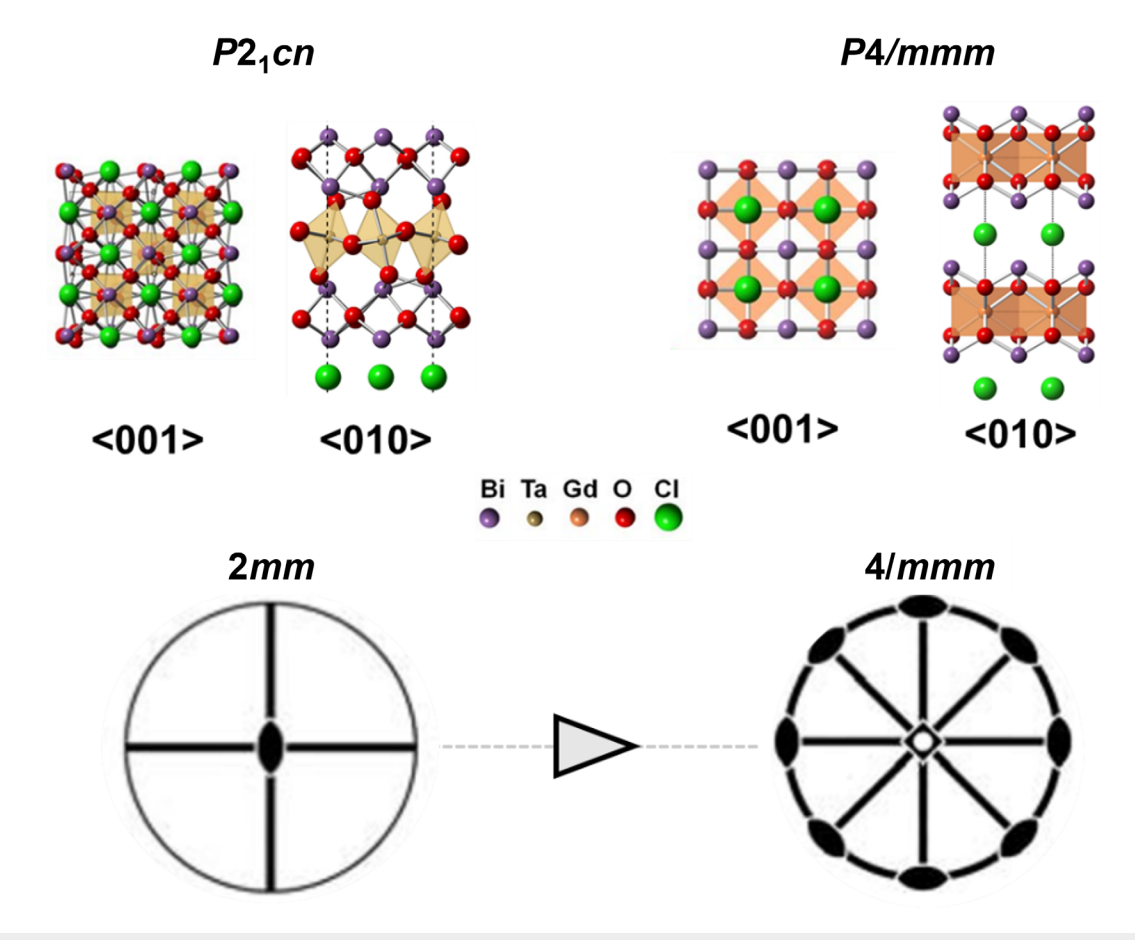


FIG. 1. Phase transformation from P2₁cn to P4/mmm represented by the respective Hermann–Mauguin notation, stereographic projections, and symmetry elements.

reflected in the HOLZ-CBED patterns through a fourfold symmetric pattern, systematic extinction rules, and well-defined HOLZ rings shown in Fig. 2. As for the lattice parameters, the change in the lattice parameter depends on factors, such as atomic positions, bonding, and external conditions, like temperature or pressure.¹³

In general, the change in lattice parameters during a phase transition depends on the interplay between the energetics of the crystal structure and the external conditions. It is important to note that the transformation from P2₁cn (orthorhombic) to P4/mmm (tetragonal) involves a change in the unit cell shape. In the orthorhombic system, the lattice parameters a, b, and c are unequal and the angles between them are 90° . In the tetragonal system, the lattice parameters a and b are equal (a = b), and the c lattice parameter may be different, with all angles still at 90°. Consequently, the relative dimensions of the unit cell along the $\langle 001 \rangle$ direction (c-axis) could either increase, decrease, or remain the same, depending on the specific material and transformation details. The c-parameter for the P21cn phase decreased from 28.808 to 28.524 Å for Ta 100% to Ta 25%, whereas the *c*-parameter increased for the P4/mmm phase from 8.951 to 8.992 Å for Ta 0% to Ta 75% as observed in our previous report by pair distribution function analysis. ¹⁴ The changes in crystal symmetry $(P2_1cn \rightarrow P4/mmm)$ when moving from higher Ta content to lower Ta content also

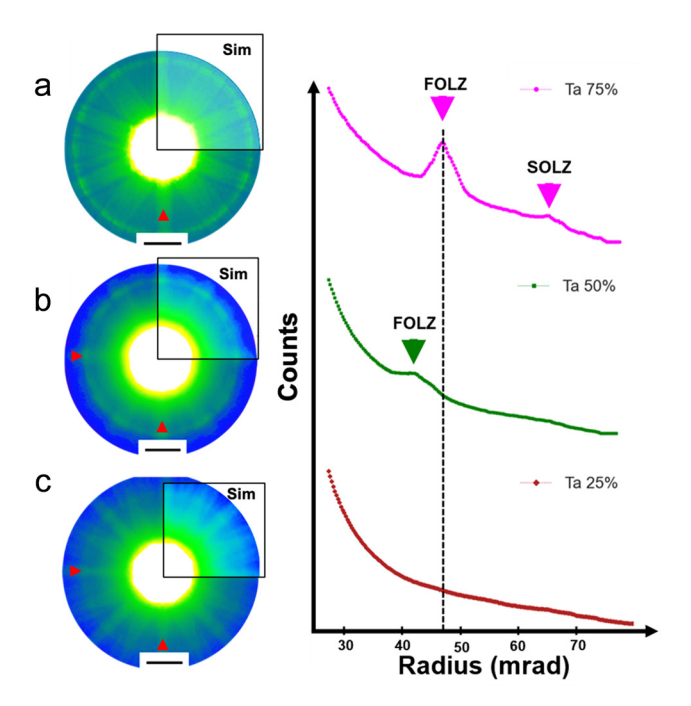


FIG. 2. Scanning transmission electron microscopy–CBED of the $\rm Bi_4 TaO_8 Cl-Bi_2 GdO_4 Cl$ intergrowths along the $\langle 001 \rangle$ direction for (a) Ta 75%, (b) Ta 50%, and (c) Ta 25%. Scale bars—20 mrad. The respective annular averages of the CBED patterns are shown next to each pattern as a 2D plot dataset with electron counts as a function of scattering angle in mrad. Arrowheads show the position of first and second order Laue zone (FOLZ and SOLZ) rings. Note that for the sample with Ta 50%, only FOLZ ring is present while for the sample with Ta 25% FOLZ and SOLZ rings are fainted in the range shown here and closer to the central CBED disk as consequence of the phase changing. Arrows in (a)–(c) indicate the mirror symmetry in the $\langle 001 \rangle$ projection.

manifest with the reduced degree of $[TaO_6]$ octahedral tilting in the crystal structure. ¹⁵

Combining UPS data with UV-visible DRS results, the band structure of photocatalysts with conduction band (CB), VB, Fermi energy ($E_{\rm F}$), and trapping states can be revealed. In addition, the work function (φ) can be determined by Eq. (1). The work function equals the difference between vacuum energy (E_0) and $E_{\rm F}$. The work function can be calculated experimentally by the difference between incident photon energy and secondary cutoff energy,

$$\varphi = E_0 - E_F = h\nu - E_{cutoff}. \tag{1}$$

The UPS results of the intergrowth and pristine samples are shown in Figs. 3(a) and 3(b). Figure 3(a) shows the secondary electron cutoff region of the samples and an Au plate reference. The work function for the Au plate was estimated to be 5.13 eV, which is in accordance with literature reports. ¹⁶ The obtained Fermi energy levels (E_F) for the intergrowths were -3.95, -3.88, -4.11, -3.92, and -4.09 eV with respect to vacuum for the Ta 0%, 25%, 50%, 75%, and 100% samples, respectively. The secondary cutoff of the Ta 50% and 100% samples had higher binding energies than the Ta 0%, Ta 25%, and Ta 75% samples, resulting in a higher work function value. UPS spectra of the VB region for the prepared samples are shown in Fig. 3(b). The obtained valence band energies (E_{VB}) relative to E_F were -6.28, -6.31, -6.43, -6.31, and -6.54 eV with respect to vacuum for the Ta 0%, 25%, 50%, 75%, and 100% samples, respectively. The E_{VB} values obtained for the samples are more negative than conventional oxides, such as TiO2 (2.9 V) or WO3 (3.0 V) vs SHE, which indicates efficient water oxidation capability and corroborates our previous findings and other reports. 9,14,17 This observation suggests significant hybridization of Bi 6s and O 2p orbitals in the VB region in accordance with the revised lone pair model, as revealed by the density of states results in our previous reports.9

The positions of the E_{VB} (determined from UPS) and the bandgap (E_σ) values (determined from UV-visible DRS measurements) reveal the overall band structures for the intergrowths and parent samples, as shown in Fig. 3(c). The bandgap values obtained from DRS measurements were 2.48, 2.45, 2.41, 2.38, and 2.34 eV for the Ta 100%, 75%, 50%, 25%, and 0% samples, respectively, with the original data reported in our previous manuscript. The energies of the conduction bands (E_{CB}) were estimated from the observed E_{VB} and E_{g} values for every sample. The experimentally obtained E_F and E_{VB} values from UPS measurements were converted into electrochemical potential values relative to the SHE, assuming an energy level value of -4.44 eV vs vacuum for the SHE. 18 This conversion helps in comparing the redox properties of the samples relative to the water splitting and CO₂ reduction potentials. Notably, all the intergrowths exhibited variable E_{VB} and E_{CB}, demonstrating the band structure engineering capability by intergrowth formation. Also, the E_{VB} and E_{CB} straddled the potentials for the OER, hydrogen evolution reaction, and CO₂ reduction reactions. Finally, EELS was used to analyze the electronic structure of these samples as discussed next.

The bandgap of the Ta 25%, Ta 50%, and Ta 75% samples was evaluated using low-loss EELS as shown in Fig. 4. The recorded bandgaps were calculated to be 2.33, 2.40, and 2.52 eV for Ta 25%, Ta 50%, and Ta 75%, respectively. The results display a clear trend: an increase in the Ta content corresponds to a larger bandgap. Notably, this variation in bandgap correlates with changes in the crystal structure of the

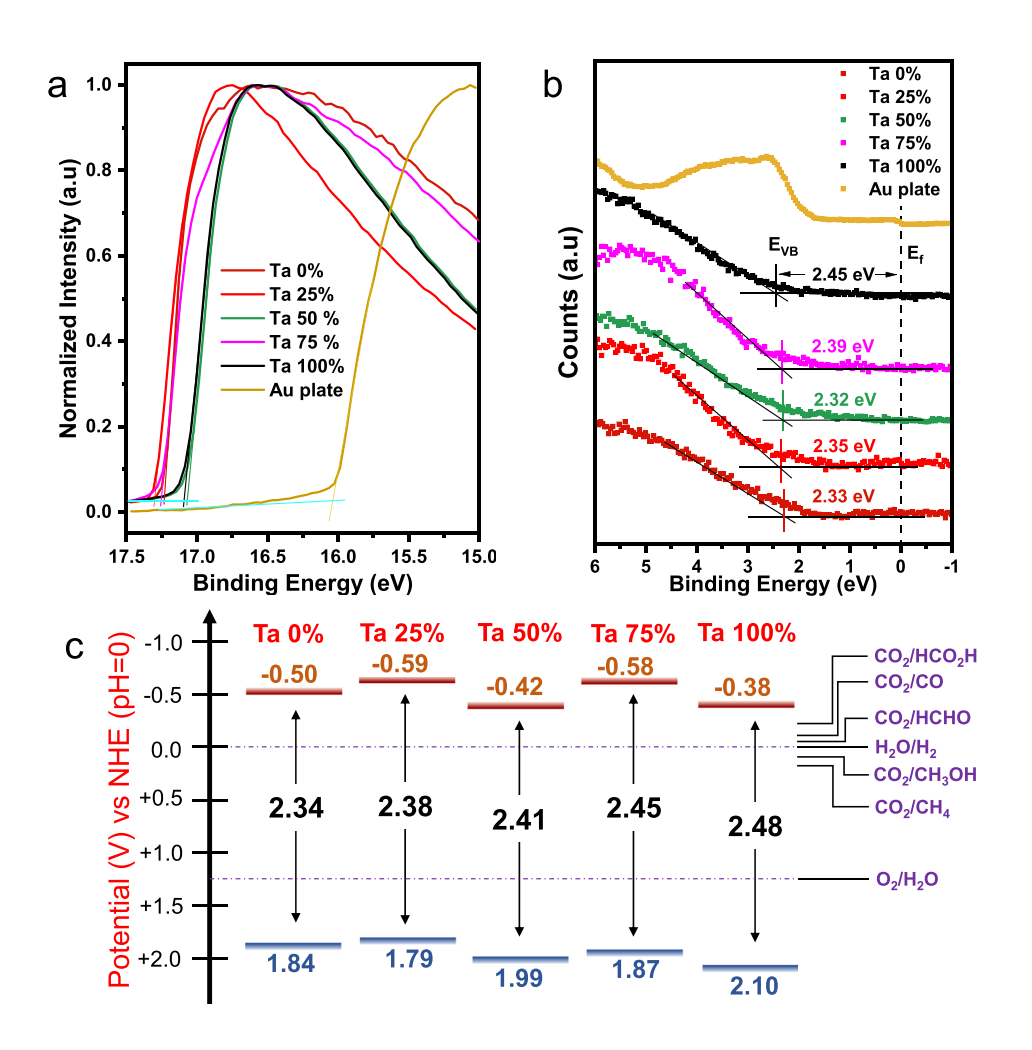


FIG. 3. UPS spectra in the (a) secondary electron cutoff region and (b) valence band region for the samples. The samples were drop-cast on an Au plate and was calibrated based on the Au plate as a reference. (c) Band alignments of the intergrowths and parent compounds with respect to different redox potentials. The E_{VB} and E_{CB} potential (V vs SHE) are estimated from UPS and bandgap measurements assuming an energy level value of $-4.44\,\mathrm{eV}$ vs vacuum for the SHE.

samples. For higher Ta content, the crystal structure was found to be $P2_1cn$, whereas a shift to the P4/mmm structure was observed for lower Ta content. This structural transition could be linked to the tilting of the $[TaO_6]$ octahedra and modulation of the c-parameter as seen in the CBED studies, and hence the bandgap, of these materials. $^{19-21}$

Moreover, the trend and $\rm E_{\rm g}$ values obtained from EELS are in accordance with and corroborate the trend and $\rm E_{\rm g}$ values obtained by DRS. Such agreement between the ensemble measurement (bulk) and the nanoscale provides evidence for nanoscale homogeneity. The changes in the material's electronic properties occur owing to the shift from the $P2_1cn$ to the P4/mmm structure, associated with the decreasing Ta content. Thus, resulting in altered charge carrier dynamics, impacting the separation and recombination rates of electron–hole pairs, which is a crucial parameter affecting photocatalytic efficiency as observed in previous reports. ^{9,14} These results were consistent with findings from UPS and underscore the importance of understanding the intricate interplay between composition, structure, and properties in these complex materials as well as unifying bulk and nanoscale measurements.

In summary, this work shows that the optoelectronic properties of Bi₄TaO₈Cl-Bi₂GdO₄Cl intergrowths can be fine-tuned by altering

their crystal structures as a function of intergrowth stoichiometry. The high spatial resolution of CBED enabled accurate determination of the positions of HOLZ rings, providing a direct evidence of symmetry changes in the intergrowths when varying the Ta content. In Bi₄TaO₈Cl-Bi₂GdO₄Cl intergrowths, stoichiometry affects [TaO₆] octahedra tilting and the electronic structure of photocatalysts. UPS and DRS measurements were used to determine conduction and valence band levels. Greater tilting of [TaO₆] results in a larger bandgap, which modulates energy levels of the bands. Furthermore, a strong correlation between bandgap determined by bulk scale (DRS) and nanoscale (EELS) techniques were observed for the intergrowth oxyhalides, providing evidence of nanoscale homogeneity. The observed intergrowth compositional tuning impacts electronic and nanoscale structure, offering a framework for designing metal octahedral photocatalysts with desired optoelectronic properties. Overall, this manuscript provides an integrated approach that establishes the bandgap energy increases with increasing Ta content, which is correlated with the crystal symmetry and the degree of [TaO₆] octahedra tilting. The modular nature of intergrowth provides building block layers to tune this structural feature for precise control of optoelectronic properties at nanoscale.

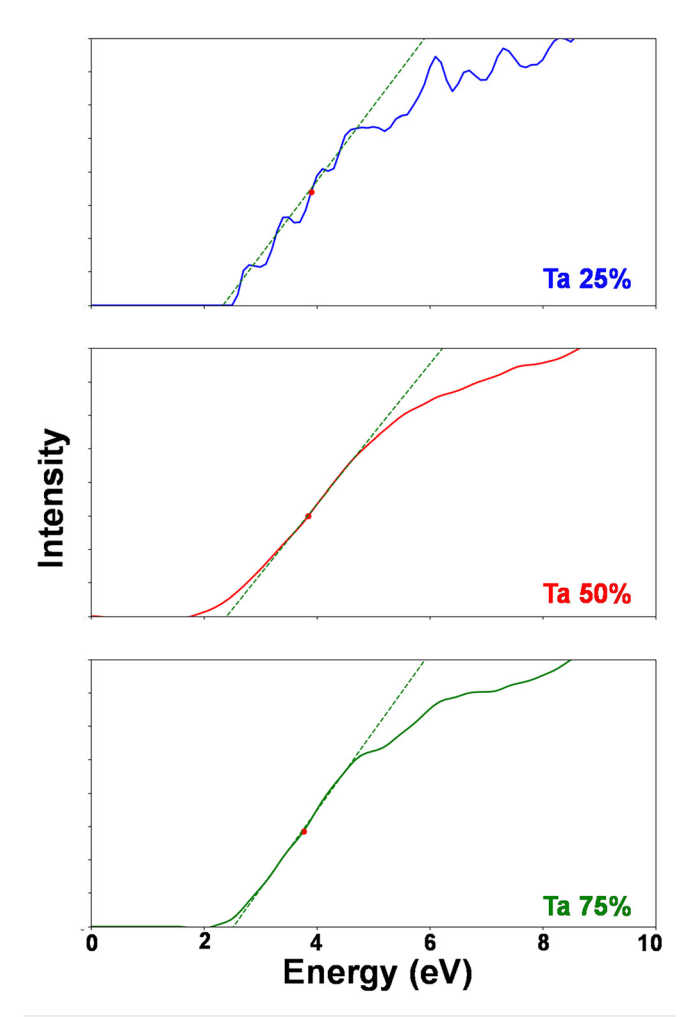


FIG. 4. The low-loss region of EELS shows the bandgap extrapolation for the Ta 25%, Ta 50%, and Ta 75% intergrowth samples.

See the supplementary material for experimental details including synthesis of samples and material characterization/instrumentation.

This work used funding support for K.C., J.S., and S.E.S. from U.S. NSF Division of Material Research SSMC 2113536 and Indiana University. We also want to thank the IU Electron Microscopy Center and Nanoscale Characterization Facility for access to the necessary instrumentation. K.C. acknowledges the Raymond Siedle Fellowship and Carroll Family Fellowship support from Dept. of Chemistry, Indiana University. This work also was enabled with funding support for R.d.R. and V.P.D. from U.S. NSF Division of Material Research (NSF Grant No. DMR-1929356—Program Manager: Lynnette Madsen). This work made use of the EPIC facility of Northwestern University's NUANCE Center, which has received support from the SHyNE Resource [National Science Foundation (NSF) Grant No. ECCS-2025633], Northwestern's MRSEC program (NSF Grant No. DMR-1720139), the Keck Foundation, and the State of Illinois through IIN.

AUTHOR DECLARATIONS Conflict of Interest

The authors have no conflicts to disclose.

Author Contributions

Kaustav Chatterjee: Conceptualization (lead); Data curation (equal); Formal analysis (equal); Funding acquisition (lead); Methodology (equal); Project administration (equal); Resources (equal); Supervision (lead); Writing - original draft (equal); Writing - review & editing (equal). Jared Stanley: Conceptualization (supporting); Data curation (supporting); Formal analysis (supporting); Methodology (supporting); Writing - original draft (supporting); Writing - review & editing (supporting). Vinayak P. Dravid: Data curation (supporting); Resources (supporting); Supervision (supporting); Writing - review & editing (supporting). Roberto dos Reis: Conceptualization (equal); Data curation (equal); Formal analysis (equal); Methodology (equal); Resources (supporting); Supervision (supporting); Writing - original draft (equal); Writing - review & editing (equal). Sara E. Skrabalak: Conceptualization (equal); Data curation (equal); Formal analysis (equal); Funding acquisition (lead); Methodology (equal); Project administration (equal); Resources (equal); Supervision (lead); Writing - original draft (equal); Writing - review & editing (equal).

DATA AVAILABILITY

The data that support the findings of this study are available from the corresponding authors upon reasonable request.

REFERENCES

- ¹Q. Wang and K. Domen, "Particulate photocatalysts for light-driven water splitting: Mechanisms, challenges, and design strategies," Chem. Rev. 120, 919–985 (2020).
- ²A. Miyoshi and K. Maeda, "Recent progress in mixed-anion materials for solar fuel production," Sol. RRL 5, 2000521 (2021).
- ³H. Fujito, H. Kunioku, D. Kato, H. Suzuki, M. Higashi, H. Kageyama, and R. Abe, "Layered perovskite oxychloride Bi₄NbO₈Cl: A stable visible light responsive photocatalyst for water splitting," J. Am. Chem. Soc. **138**, 2082–2085 (2016).
- ⁴D. Kato, K. Hongo, R. Maezono, M. Higashi, H. Kunioku, M. Yabuuchi, H. Suzuki, H. Okajima, C. Zhong, K. Nakano, R. Abe, and H. Kageyama, "Valence band engineering of layered bismuth oxyhalides toward stable visible-light water splitting: Madelung site potential analysis," J. Am. Chem. Soc. 139, 18725–18731 (2017).
- ⁵K. Chatterjee, M. Banoo, S. Mondal, L. Sahoo, and U. K. Gautam, "Synthesis of Bi₃TaO₇–Bi₄TaO₈Br composites in ambient air and their high photocatalytic activity upon metal loading," Dalton Trans. **48**, 7110–7116 (2019).
- ⁶K. Chatterjee and S. E. Skrabalak, "Durable metal heteroanionic photocatalysts," ACS Appl. Mater. Interfaces 13, 36670–36678 (2021).
- 7D. Kato, O. Tomita, R. Nelson, M. A. Kirsanova, R. Dronskowski, H. Suzuki, C. Zhong, C. Tassel, K. Ishida, Y. Matsuzaki, C. M. Brown, K. Fujita, K. Fujii, M. Yashima, Y. Kobayashi, A. Saeki, I. Oikawa, H. Takamura, R. Abe, H. Kageyama, T. E. Gorelik, and A. M. Abakumov, "Bi₁₂O₁₇Cl₂ with a sextuple Bi–O layer composed of rock-salt and fluorite units and its structural conversion through fluorination to enhance photocatalytic activity," Adv. Funct. Mater. 32, 2204112 (2022).
- ⁸H. Kageyama, K. Hayashi, K. Maeda, J. P. Attfield, Z. Hiroi, J. M. Rondinelli, and K. R. Poeppelmeier, "Expanding frontiers in materials chemistry and physics with multiple anions," Nat. Commun. 9, 772 (2018).
- ⁹K. Chatterjee, R. dos Reis, J. K. Jarada, J. K. Mathiesen, S. L. A. Bueno, K. M. Ø. Jensen, J. M. Rondinelli, V. Dravid, and S. E. Skrabalak, "Durable multimetal

- oxychloride intergrowths for visible light-driven water splitting," Chem. Mater. 33, 347–358 (2021).
- ¹⁰S. Balaz, S. H. Porter, P. M. Woodward, and L. J. Brillson, "Electronic structure of tantalum oxynitride perovskite photocatalysts," Chem. Mater. 25, 3337–3343 (2013).
- ¹¹K. Chatterjee, S. Bueno, S. Skrabalak, V. Dravid, and R. dos Reis, "Nanoscale investigation of layered oxychloride intergrowth photocatalysts for visible light driven water splitting," Microsc. Microanal. 26, 376–379 (2020).
- ¹²H. J. Maier, R. R. Keller, H. Renner, H. Mughrabi, and A. Preston, "On the unique evaluation of local lattice parameters by convergent-beam electron diffraction," Philos. Mag. A 74, 23–43 (1996).
- ¹³R. Wittmann, C. Parzinger, and D. Gerthsen, "Quantitative determination of lattice parameters from CBED patterns: Accuracy and performance," Ultramicroscopy 70, 145–159 (1998).
- ¹⁴K. Chatterjee, N. P. L. Magnard, J. K. Mathiesen, K. M. Ø. Jensen, and S. E. Skrabalak, "Local structure analysis and structure mining for design of photocatalytic metal oxychloride intergrowths," J. Mater. Chem. A 10, 23212–23221 (2022).
- 15 R. dos Reis, H. Yang, C. Ophus, P. Ercius, G. Bizarri, D. Perrodin, T. Shalapska, E. Bourret, J. Ciston, and U. Dahmen, "Determination of the structural phase

- and octahedral rotation angle in halide perovskites," Appl. Phys. Lett. 112, 071901 (2018).
- ¹⁶G. N. Derry, M. E. Kern, and E. H. Worth, "Recommended values of clean metal surface work functions," J. Vac. Sci. Technol., A 33, 060801 (2015).
- ¹⁷X. Zhou and H. Dong, "Density functional studies on layered perovskite oxyhalide Bi₄MO₈X photocatalysts (M = Nb and Ta, X = Cl, Br, and I)," J. Phys. Chem. C 121, 20662–20672 (2017).
- ¹⁸S. Trasatti, "The absolute electrode potential: An explanatory note (Recommendations 1986)," Pure Appl. Chem. 58, 955–966 (1986).
- ¹⁹H. Lakner, B. Bollig, S. Ungerechts, and E. Kubalek, "Characterization of III V semiconductor interfaces by Z-contrast imaging, EELS and CBED," J. Phys. D: Appl. Phys. 29, 1767 (1996).
- ²⁰S. Yoshida, H. Akamatsu, A. S. Gibbs, S. Kawaguchi, V. Gopalan, K. Tanaka, and K. Fujita, "Interplay between oxygen octahedral rotation and deformation in the acentric ARTiO₄ series toward negative thermal expansion," Chem. Mater. 34, 6492–6504 (2022).
- ²¹R. Prasanna, A. Gold-Parker, T. Leijtens, B. Conings, A. Babayigit, H.-G. Boyen, M. F. Toney, and M. D. McGehee, "Band gap tuning via lattice contraction and octahedral tilting in perovskite materials for photovoltaics," J. Am. Chem. Soc. 139, 11117–11124 (2017).